

Ti:Er:LiNbO₃ Waveguide Laser of Optimized Efficiency

Ingo Baumann, Ralf Brinkmann, Manfred Dinand, Wolfgang Sohler, *Associate Member, IEEE*,
and Susanne Westenhöfer

Abstract— The development of a Fabry–Perot-type Ti:Er:LiNbO₃ waveguide laser of optimized CW output power up to 63 mW ($\lambda_s = 1561$ nm) at a pump power level of 210 mW ($\lambda_p = 1480$ nm) and a slope efficiency of up to 37% is reported. The theoretical model for the waveguide laser is presented and applied to determine the optimum resonator configuration using waveguide parameters obtained from a detailed characterization of the laser sample. With pulsed pumping, waveguide laser pulses of up to 6.2 W peak power were observed. Apart from residual relaxation oscillations, the laser emission proved to be shot-noise limited.

I. INTRODUCTION

IN the last few years, there has been a growing interest in rare-earth-doped, optically pumped waveguide amplifiers and lasers in LiNbO₃ [1], [2]. In particular, erbium doping is of major interest as it leads to optical amplification and lasing in the wavelength range $1520 \text{ nm} \leq \lambda \leq 1560$ nm, most important for fiber optical communication. LiNbO₃ permits the fabrication of high-quality channel guides in (locally, photolithographically defined) diffusion-doped surfaces of high erbium concentration. Moreover, LiNbO₃ has excellent electro- and acoustooptical properties. Therefore, besides CW-emitting, free-running Fabry–Perot-type waveguide-lasers [3], [4], also mode-locked [5] and tunable waveguide lasers [6] have been demonstrated. Recently, a fixed-wavelength, single-longitudinal-mode laser was realized by replacing one of the cavity mirrors by an etched Bragg-reflector grating [7], opening the possibility for integrating a laser into a more complex integrated optical circuit. All this work has been accompanied by a quantitative modeling of the laser devices to improve the understanding of all the physical phenomena involved and to allow an optimization of the laser properties [8]–[11].

In this paper, the development of a CW Fabry–Perot-type Ti:Er:LiNbO₃ waveguide laser ($\lambda_s = 1561$ nm) of optimized output power up to 63 mW at a pump power level of 210 mW ($\lambda_p = 1480$ nm) and slope efficiency up to 37% is described. In Section II, the theoretical model used to analyze the laser properties is presented. Section III deals with the technology for the fabrication of Er-doped waveguides in LiNbO₃. A detailed characterization of these active channel guides is given, yielding the input parameters

for the theoretical modeling. The optimum configuration of a Fabry–Perot-type laser based on the fabricated Ti:Er:LiNbO₃ waveguide amplifiers is discussed in Section IV, and the fabrication of the laser cavity is described. The performance of the waveguide laser under CW and pulsed pumping is the topic of Section V. To obtain a laser which is easy to handle and to operate, we pigtailed and packaged the device. Section VI presents the performance of this laser module. Furthermore, the noise characteristics of the laser emission will be discussed.

II. THEORETICAL MODELING OF Ti:Er:LiNbO₃ WAVEGUIDE LASERS

In this section, the fundamental equations for the theoretical modeling of time-independent phenomena of locally Er-doped optically pumped Ti:LiNbO₃-waveguide lasers are developed. The basic structure of these lasers are titanium-diffused optical strip waveguides, which are embedded in (locally) erbium diffusion-doped LiNbO₃ (see Fig. 1). The excitation process occurs optically by coupling external radiation ($\lambda_p \approx 1480$ nm) directly into the waveguides (longitudinally pumping). The feedback elements are realized with dielectric mirrors (with wavelength dependent reflectivities) at the waveguide endfaces.

In order to analyze the light matter interaction causing stimulated emission and optical amplification, one has to model the time-dependent population densities of the dopant ions—this will be done by time-dependent rate equations [9]—and the evolution of the guided modes through the locally doped waveguide along the propagation direction z , which can be deduced from the equation of continuity for a gain medium [12]. These equations have to be solved taking into account initial and boundary conditions.

Restricting the discussion to the 1.48- μm pumpband as the preferred absorption band in LiNbO₃—there is only a small amount of excited state absorption (ESA) (which has not yet been investigated in more detail), no photorefractive damage occurs and furthermore, monomode waveguides for both pump and signal can be fabricated leading to a good overlap with the erbium diffusion profile—a quasi-two-level-model can be used to model amplification in the wavelength range $\lambda_s \approx 1.5 \mu\text{m}$ [9]. The energy splitting of the $^4I_{15/2}$ ground state and the first excited state $^4I_{13/2}$ due to the Stark-effect is taken into account with wavelength dependent absorption and

Manuscript received December 14, 1995; revised April 16, 1996.

The authors are with Angewandte Physik, Universität-GH Paderborn, D-33098 Paderborn, Germany.

Publisher Item Identifier S 0018-9197(96)06279-3.

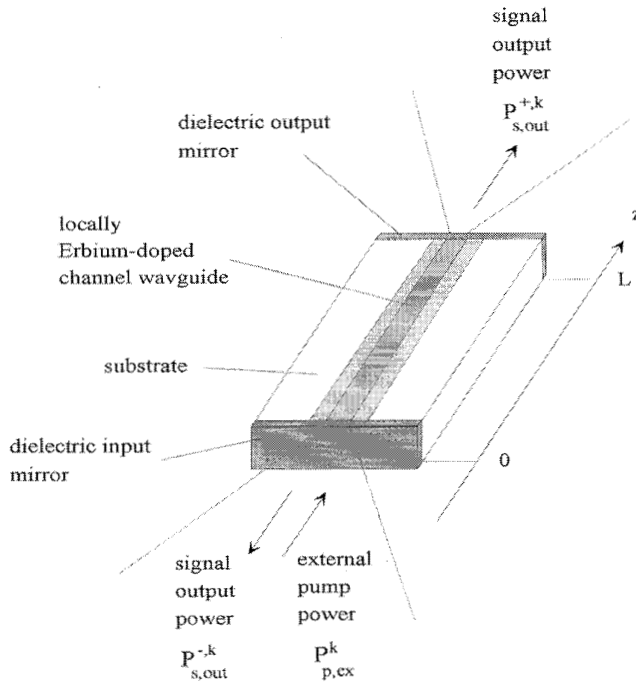


Fig. 1. Erbitium-doped integrated optical Fabry-Perot-type waveguide laser consisting of an Erbitium-doped waveguide amplifier of length L in an optical resonator formed by dielectric endface mirrors. $P_{p,ex}^k$: k -polarized ($k = \pi, \sigma$) external pump power, $P_{s,out}^{\pm,k}$: signal output power in forward (+) and backward (-) directions.

emission cross sections. $A_{21} = 1/\tau$ describes the spontaneous transition from the excited state to the ground state; τ is the fluorescence lifetime. The absorption (emission) rate from level 1 (2) to level 2 (1) is given by w_{12} (w_{21}). The w_{mn} can be written as the sum of the pump and signal absorption and emission rates W_{mn}^j , which are defined in terms of the mode intensity profiles (defined as spectral densities) $i_j(x, y, z, \lambda_j)$, the cross sections $\sigma_{mn,j}^k = \sigma_{mn}^k(\lambda_j)$ and the photon energies $h\nu_j = hc/\lambda_j$. c is the velocity of light and h Planck's constant. The index j describes contributions, which result from the pump ($j = p$) and from the signal ($j = s$), $mn = 12, 21$ represent absorption and emission processes, and $k = \pi, \sigma$ characterizes the polarization, which can be parallel ($\parallel \hat{z} \hat{=} \pi$) and perpendicular ($\perp \hat{=} \sigma$) to the optical axis of the LiNbO_3 crystal

$$w_{mn} = \sum_{j=p,s} W_{mn}^j = \sum_{j=p,s} \left(\frac{1}{hc} \sum_{k=\pi,\sigma} \int_0^\infty \lambda_j \sigma_{mn,j}^k i_j^k(x, y, z, \lambda_j) d\lambda_j \right). \quad (1)$$

The spectral densities $i_j^k(x, y, z, \lambda_j)$ can be written as a product of the intensity $I_j^k(x, y, z, \lambda_j)$ and the function $f_j^k(\lambda_j)$, describing the spectral dependence of the pump and the signal, respectively. $I_j^k(x, y, z, \lambda_j)$ itself can be split into three terms: the power $P_j^{0,k}$, the normalized transversal distribution $j_0^k(x, y, \lambda_j)$ with $\iint j_0^k(x, y, \lambda_j) dx dy = 1$, and the sum of

the forward and backward propagating intensity amplitudes $j^{\pm,k}(z)$

$$i_j^k(x, y, z, \lambda_j) = I_j^k(x, y, z, \lambda_j) f_j^k(\lambda_j) = P_j^{0,k} j_0^k(x, y, \lambda_j) (j^{+,k}(z) + j^{-,k}(z)) f_j^k(\lambda_j). \quad (2)$$

$f_s^k(\lambda_s)$ takes the possible longitudinal-mode spectrum into account. The amplitudes of the different modes—with a mode-spacing $\Delta\lambda_s = \lambda_{s,i+1} - \lambda_{s,i} = \lambda_{s,i}^2 / (2n_k(\lambda_{s,i})L)$ between two neighboring modes—are proportional to the gain spectrum, which is represented by \tilde{f}_s^k

$$f_s^k(\lambda_s) = \tilde{f}_s^k(\lambda_s) \sum_i^{N_s} \delta(\lambda_s - \lambda_{s,i}). \quad (3)$$

The functions f_j^k are normalized according to $\int_0^\infty f_j^k(\lambda_j) d\lambda_j = 1$, $j = p, s$.

The interactions between the Er^{3+} ions and the pump/signal photons can be described with the following rate equations [9]

$$\frac{dN_1}{dt} = -\frac{dN_2}{dt} = -w_{12}N_1 + (w_{21} + A_{21})N_2. \quad (4)$$

$N_1(x, y, z, t)$ ($N_2(x, y, z, t)$) is the population density of the ground state (excited state). The sum of both is the total erbium concentration profile $N_0(x, y) = N_1(x, y, z, t) + N_2(x, y, z, t)$, which is independent of the coordinate z and the time t . Considering the steady state, all time derivatives in (4) can be neglected. Then N_1 and N_2 can be written as

$$N_1 = \frac{w_{21} + A_{21}}{w_{12} + w_{21} + A_{21}} N_0 \quad (5)$$

$$N_2 = \frac{w_{12}}{w_{12} + w_{21} + A_{21}} N_0. \quad (6)$$

The evolution of the pump and the signal intensity amplitudes $j^{\pm,k}(z, t)$ along the propagation direction z can be deduced from the equation of continuity for a gain medium [12]. In the steady state, time dependencies can be neglected and the following system of coupled ordinary differential equations for the forward (+) and backward (-) running waves can be obtained:

$$\frac{dj^{\pm,k}(z)}{dz} = \pm \gamma_j^k(z, \lambda_j) j^{\pm,k}(z) \quad (7)$$

with

$$\gamma_j^k(z, \lambda_j) = -\tilde{\alpha}_j^k + \iint (\sigma_{21,j}^k N_2 - \sigma_{12,j}^k N_1) j_0^k dx dy. \quad (8)$$

The term $\tilde{\alpha}_j^k$ describes the waveguide scattering losses, $\sigma_{12,j}^k N_1$ losses by absorption, and $\sigma_{21,j}^k N_2$ winnings by stimulated emission. The integration has to be carried out over the waveguide cross section taking into account the overlap of the normalized transversal intensity distributions $j_0^k(x, y, \lambda_j)$ with the space-dependent population densities N_1 and N_2 , which are themselves proportional to the erbium concentration profile N_0 [see (5) and (6)].

In addition to (5)–(8), boundary conditions have to be fulfilled at $z = 0$ and $z = L$

$$\begin{aligned} p^{+,k}(0) &= R_1^p p^{-,k}(0) + \frac{P_{p,\text{ex}}^k}{P_c^{0,k}} [1 - R_1^p] \epsilon_p^k \\ p^{-,k}(L) &= R_2^p p^{+,k}(L) \\ s^{+,k}(0) &= R_1^s s^{-,k}(0) \\ s^{-,k}(L) &= R_2^s s^{+,k}(L) \end{aligned} \quad (9)$$

$R_1^j = R_1(\lambda_j)$ and $R_2^j = R_2(\lambda_j)$ are the (wavelength dependent but polarization independent) reflectivities of the front and rear mirror, respectively. $P_{p,\text{ex}}^k$ is the external pump power, and $P_c^{0,k}$ ($P_s^{0,k}$) the pump (signal) power within the resonator with an evolution along the propagation direction described by $p^{\pm,k}(z)$ ($s^{\pm,k}(z)$). The (polarization dependent) pump-coupling efficiency has been taken into account with the term ϵ_p^k . The forward and backward signal output power can be written as

$$\begin{aligned} P_{s,\text{out}}^{+,k} &= (1 - R_2^s) s^{+,k}(L) P_s^{0,k} \\ P_{s,\text{out}}^{-,k} &= (1 - R_1^s) s^{-,k}(0) P_s^{0,k}. \end{aligned} \quad (10)$$

Using the expression

$$\begin{aligned} \frac{d(j^{+,k} j^{-,k})}{dz} &= j^{+,k} \frac{dj^{-,k}}{dz} + \frac{dj^{+,k}}{dz} j^{-,k} \\ &= j^{+,k} (-\gamma_j^k j^{-,k}) + \gamma_j^k j^{+,k} j^{-,k} = 0 \quad \forall z \end{aligned} \quad (11)$$

the boundary value problem (5)–(9) can be reduced to an initial value problem for the forward running intensity amplitudes $j^{+,k}(z)$ [13, p. 146]

$$\begin{aligned} \frac{ds^{+,k}(z)}{dz} &= \gamma_s^k(z, \lambda_s) s^{+,k}(z) \\ \frac{dp^{+,k}(z)}{dz} &= \gamma_p^k(z, \lambda_p) p^{+,k}(z) \\ s^{-,k}(z) &= \frac{1}{R_1^s} \frac{[s^{+,k}(0)]^2}{s^{+,k}(z)} \\ p^{-,k}(z) &= \frac{1}{R_1^p} \frac{[p^{+,k}(0)]^2}{p^{+,k}(z)} \left(1 - \frac{P_{p,\text{ex}}^k [1 - R_1^p] \epsilon_p^k}{P_c^{0,k} p^{+,k}(0)} \right). \end{aligned} \quad (12)$$

If the amplitudes $j^{+,k}$ at $z = 0$ are set to 1, for a given external pump power $P_{p,\text{ex}}^k$ the powers $P_s^{0,k}$ and $P_c^{0,k}$ have to be determined self-consistently from (12).

The diagrams of Fig. 2 show the evolution of the pump and signal intensity amplitudes versus the propagation direction z in a typical resonator. Both mirrors have a high reflectance for the signal wavelength whereas the input (output) coupler for the pump wavelength has been chosen to be high (low). This configuration leads to a double-pass for the pump, which increases the pump efficiency and therefore improves the threshold pump power as well as the slope efficiency and the signal output power. As can be seen from the upper left diagram, the forward-running pump intensity amplitude ($p^{+,k}$) decreases along z , is reflected at $z = L$, becomes $p^{-,k}$, the backward-running pump intensity amplitude, which itself decreases along $-z$. $s^{+,k}$ ($s^{-,k}$) increases along z ($-z$), respectively (see lower left diagram). At $z = 0$ and $z = L$,

the boundary conditions (9) are fulfilled. Additionally, to $j^{\pm,k}$ ($j = p, s$) both the sums $j^{+,k} + j^{-,k}$ and the products $j^{+,k} \cdot j^{-,k}$ are shown in the right diagrams of Fig. 2. It can be seen that, as expected from (11), the products are constant along z . Furthermore, the sums also can be considered in a good approximation as constants. This behavior has been used to theoretically model the time-dependent waveguide laser phenomena [11].

With (11) and (12), the signal output powers can be written as

$$\begin{aligned} P_{s,\text{out}}^{+,k} &= \frac{1 - R_2^s}{\sqrt{R_1^s R_2^s}} P_s^{0,k} \\ P_{s,\text{out}}^{-,k} &= \frac{1 - R_1^s}{R_1^s} P_s^{0,k}. \end{aligned} \quad (13)$$

The power characteristics $P_{s,\text{out}}^{\pm,k}(P_{p,\text{ex}}^k)$ of the laser can be modeled by varying $P_{p,\text{ex}}^k$, leading in solid-state lasers to the typical linear behavior. At the threshold pump power, the total laser losses (waveguide scattering losses and losses due to the reflection at the dielectric mirrors) are compensated by the gain; laser operation sets in.

The (external) slope efficiency is defined as

$$\eta_{\text{ex}}^{\pm,k} = \frac{dP_{s,\text{out}}^{\pm,k}}{dP_{p,\text{ex}}^k}, \quad (14)$$

the quotient

$$Q_{\text{ex}}^{\pm,k} = \frac{h\nu_p P_{s,\text{out}}^{\pm,k}}{h\nu_s P_{p,\text{ex}}^k} \quad (15)$$

as (external) quantum efficiency. With (14) and (15) and with $P_{p,\text{ex}}^{\text{th},k}$ as the (external) threshold power, the signal output powers can be expressed as

$$P_{s,\text{out}}^{\pm,k} = \eta_{\text{ex}}^{\pm,k} (P_{p,\text{ex}}^k - P_{p,\text{ex}}^{\text{th},k}). \quad (16)$$

III. Ti:Er:LiNbO₃ WAVEGUIDE FABRICATION AND CHARACTERIZATION

A. Erbium Diffusion Doping and Waveguide Fabrication

\hat{Z} -cut LiNbO₃ was used as a substrate to take advantage of the higher erbium diffusivity in this crystal orientation. The activation energies E_a and diffusion constants D_0 parallel (perpendicular) to the c -axis are $E_a = 2.28$ (2.44) eV, $D_0 = 4.8 \cdot 10^{-5}$ ($12.0 \cdot 10^{-5}$) cm²/s [14]. The diffusion temperature was set to 1130 °C, slightly below the Curie temperature. The high diffusion temperature accelerates the erbium indiffusion and increases the erbium solubility in LiNbO₃ which varies exponentially with temperature

$$c_{\text{Er,max}} = c_0 \exp(-H_s/k_B T)$$

with $c_0 = 1.8 \cdot 10^{25}$ cm⁻³, the heat of solution $H_s = 1.36$ eV and k_B being Boltzmann's constant [14]. Therefore, the maximum erbium concentration at 1130 °C is $2.3 \cdot 10^{20}$ cm⁻³, corresponding to the solubility limit. A sufficient overlap of erbium concentration profile and intensity of the guided modes is obtained for diffusion times of about 100 h. Both parameters (diffusion temperature and time) determine the

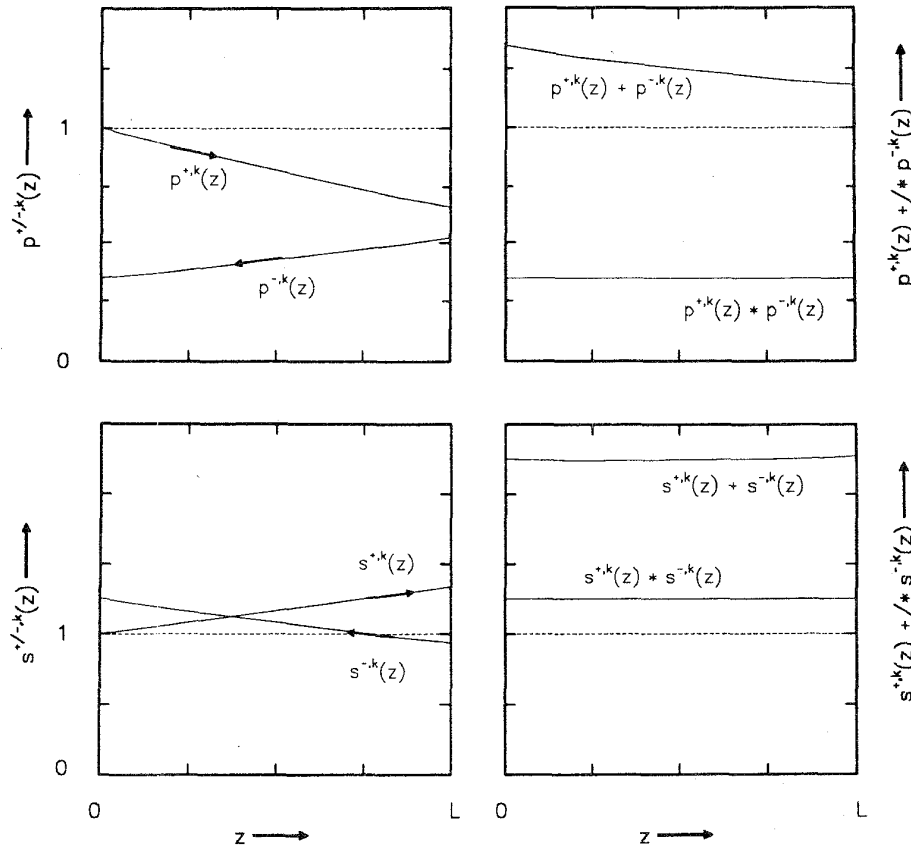


Fig. 2. Typical evolution along the propagation direction z of the forward- (+) and backward- (-) running pump ($p^{\pm,k}$) (upper left) and signal ($s^{\pm,k}$) (bottom left) intensity amplitudes in a Fabry-Perot-type waveguide laser. Additionally, the sums ($p^{+,k} + p^{-,k}$) and ($s^{+,k} + s^{-,k}$) (upper right) as well as the products ($p^{+,k} \cdot p^{-,k}$) and ($s^{+,k} \cdot s^{-,k}$) (bottom right) are shown [compare (11)].

maximum thickness of 27.5 nm of a metallic erbium layer, and in this way the maximum number of erbium atoms, which can be incorporated in the LiNbO_3 substrate. However, the high concentration near the solubility limit leads to a slight increase of the waveguide scattering losses. We therefore decided to reduce the erbium layer thickness to 22 nm to get a nearly Gaussian concentration profile with a surface concentration of $1.35 \cdot 10^{20} \text{ cm}^{-3}$ and a $1/e$ -depth of 6 μm .

The erbium layer was deposited on the substrate surface using e -beam evaporation. Only one half of the wafer was covered with erbium to allow also the fabrication of undoped waveguides on the same substrate for comparison and additional characterization. The diffusion was performed at 1130 $^\circ\text{C}$ in a dry Argon atmosphere, but in flowing oxygen during heating up and cooling down. Afterwards, optical waveguides were fabricated by indiffusion of 6- μm -wide and 95-nm-thick titanium stripes at 1030 $^\circ\text{C}$ within 9 h. Finally, the waveguide endfaces were carefully polished perpendicular to the waveguide axis.

B. Ti:Er:LiNbO₃ Waveguide Characterization

To get a complete set of input parameters for the theoretical modeling, the Ti:Er:LiNbO₃ samples were characterized in detail.

At first, the erbium doping profile was investigated. Standard techniques for this purpose, such as secondary ion mass spectroscopy (SIMS) or secondary neutral mass spectroscopy (SNMS), do not have the spatial resolution which would be necessary to analyze the two-dimensional concentration profile in the region of the titanium indiffused strip waveguides. Therefore, one-dimensional profiles of samples fabricated by planar doping together with the laser chip were measured by SNMS as described in [14]. The resulting erbium profile in the titanium codiffused region was used for the modeling as a reasonable approximation of the true two-dimensional distribution. The results of the experimental investigations are shown in Fig. 3. Four doping profiles were investigated: the erbium doping profile after 1130 $^\circ\text{C}/100$ h diffusion and after 1130 $^\circ\text{C}/100$ h + 1030 $^\circ\text{C}/9$ h diffusion (a) (the second diffusion step corresponds to the annealing during titanium indiffusion), (b) the erbium doping profile in the titanium doped region, and (c) the titanium doping profile in the codoped region. The erbium doping profiles in the pure erbium doped region after the first diffusion step and after the following annealing during titanium indiffusion are identical and nearly Gaussian-like. The latter is shown in region (a) of Fig. 3. No detectable change of the erbium distribution was observed due to the second annealing step.

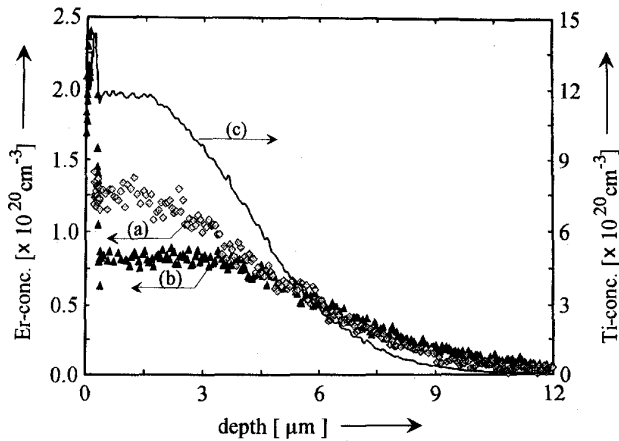


Fig. 3. Erbium and titanium concentration profiles versus depth measured by SNMS: (a) Er-profile after indiffusion (22 nm, 1130 °C, 100 h, \hat{Z} -cut) and annealing (1030 °C, 9 h). (b) The same as before, but with additional Ti-indiffusion during annealing instead of annealing. (c) Corresponding titanium distribution (95 nm, 1030 °C, 9 h).

However, the erbium doping profile in the titanium ‘codoped’ region was modified considerably: close to the surface of the substrate an erbium enrichment occurs, whereas up to a 3- μm depth the erbium concentration has a nearly constant level of about $0.8 \cdot 10^{20} \text{ cm}^{-3}$. This effect is still under investigation, but from preliminary results we suggest that this is due to a titanium induced segregation, reducing the erbium solubility and increasing the erbium diffusivity. A more detailed description of these investigations will be presented elsewhere. The erbium solubility at 1030 °C is $0.99 \cdot 10^{20} \text{ cm}^{-3}$, lower than the surface concentration of the erbium profile in region (a). Therefore, the sample doped at 1130 °C as described above can be considered as supersaturated at 1030 °C, but pure annealing at this temperature is not sufficient to stimulate segregation. Also, the titanium profile of region (c) shows the formation of a titanium enrichment near the surface with approximately the same depth as the erbium enrichment. The formation of an $\text{Er}_x\text{Ti}_y\text{Nb}_z\text{O}$ -surface compound seems to be probable. This segregation effect can be avoided (or at least considerably reduced) by titanium indiffusion at ≥ 1060 °C.

The optical characterization of the Ti:Er:LiNbO₃ waveguides proved that the channels are single-moded with intensity distributions of $5.8 \mu\text{m} \times 3.9 \mu\text{m}$ ($\sigma \hat{=} \text{TE}$) and $4.0 \mu\text{m} \times 2.3 \mu\text{m}$ ($\pi \hat{=} \text{TM}$) full widths at half maximum (fwhm) parallel \times perpendicular to the surface of the substrate ($\lambda = 1545 \text{ nm}$). The mode fields considered in the theoretical modeling were fitted to the measured halfwidths.

Results of small-signal absorption/gain measurements in the 70-mm-long sample, carried out as described in [15], are shown in Fig. 4 for $\sigma \hat{=} \text{TE}$ -polarized pump and signal radiations. As pump source, a fiber coupled color center laser (CCL) was used. On the left-hand side, the signal transmission through the doped waveguides (including absorption/gain and scattering losses, but not coupling losses) is given versus coupled pump power for several signal wavelengths and, on the right-hand side, versus signal wavelength for different levels of coupled pump power.

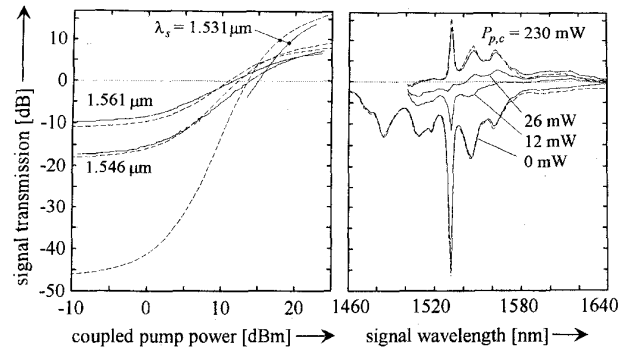


Fig. 4. Optical amplifier performance of the Er:Ti:LiNbO₃ waveguide. Left-hand side: Signal transmission in dB versus coupled pump power in dBm for several signal wavelengths. Right-hand side: Signal transmission in dB versus signal wavelength in nm for different levels of coupled pump power (pump and signal $\sigma \hat{=} \text{TE}$ -polarized; pump wavelength $\lambda_p = 1.484 \mu\text{m}$; resolution of the measurement: 0.5 nm). Solid lines: Experimental, dashed lines: Calculated data.

Without pumping ($P_{p,c} = 0 \text{ mW}$), the maximum absorption is observed at a wavelength of 1531 nm. The absorption band around 1480 nm can be used for optical pumping. It is relatively broad ($\Delta\lambda \approx 20 \text{ nm}$) and therefore allows efficient pumping with high-power laser diodes, which have a typical bandwidth of 10 nm. Further absorption bands are found around 1546 nm and 1561 nm. The absorption spectrum for $\pi \hat{=} \text{TM}$ -polarized signal radiation—not shown here—looks very similar with additional, but weak absorption features at 1575 nm and about 1600 nm.

With the knowledge of the absorption α_{eff} and the total losses α_{tot} measured with the resonator technique [16], the scattering losses $\tilde{\alpha}$ can be determined via $\tilde{\alpha} = \alpha_{\text{tot}} - \alpha_{\text{eff}}$. Values of 0.18 dB/cm and 0.25 dB/cm are found for $\sigma \hat{=} \text{TE}$ - and $\pi \hat{=} \text{TM}$ -polarized radiation, respectively, showing a small increase in comparison to the typical figures of the undoped waveguides on the same sample: 0.04 dB/cm for σ - and 0.14 dB/cm for π -polarized light.

In the pumped waveguides, the threshold for a signal transmission of 0 dB decreases with increasing wavelength due to electronic transitions to the upper, less populated sublevels of the ground-state manifold of the Er^{3+} -ions, which facilitates population inversion. With a coupled pump power of 22.8 dBm ($\hat{=} 190 \text{ mW}$; coupling efficiency $\sim 85\%$) up to 13.8-dB signal amplification is obtained ($\lambda_s = 1531 \text{ nm}$) in a single pass of signal and pump within the 7-cm-long sample. The maximum gain for $\pi \hat{=} \text{TM}$ -polarized pump and signal radiations is smaller (e.g., 11.1 dB at $P_{p,c} = 21.9 \text{ dBm}$; $\lambda_s = 1531 \text{ nm}$) due to the higher scattering losses and smaller emission cross sections in this configuration.

The calculated data based on the model presented in [9] are included in Fig. 4 as dashed curves. The modeled absorption spectrum and the gain spectrum for a coupled pump power of 230 mW show an almost quantitative agreement with the measured graphs. A fairly good agreement of the theoretically predicted and experimentally observed dependence of the signal transmission on the pump power is obtained at least for coupled pump powers below $\sim 10 \text{ dBm}$. When raising the

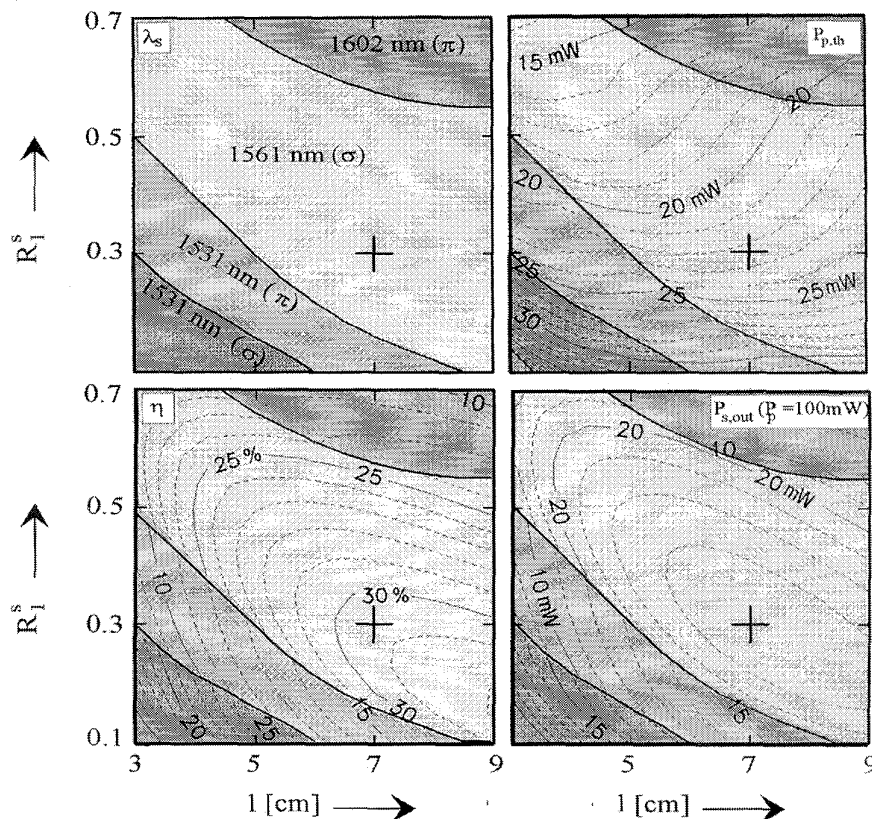


Fig. 5. Calculated performance of a laser with the amplifier described in Section III as active medium in dependence of the resonator length and input/output-coupler reflectivity R_1^s . Pump: $\lambda_p = 1484$ nm, σ -polarization. Upper left: Emission wavelength and polarization of the waveguide laser. Upper right: Threshold pump power. Lower left: Slope efficiency. Lower right: Output power at $P_{p,inc} = 100$ mW.

pump power beyond this level, the discrepancy between calculated and measured data at first increases and then decreases again at power levels above ~ 20 dBm. This behavior may be explained by upconversion processes not taken into account in the calculations [13, p. 108].

IV. LASER CAVITY DESIGN

With the knowledge of the doped waveguide parameters as input data, it is possible to theoretically model the optimum resonator configuration to obtain a waveguide laser with maximum output power.

Some predictions can be made before starting the calculations. To have the complete output power from the laser only in one direction, one of the mirrors forming the cavity has to be a 100% reflector for the waveguide laser emission. As the laser will be pumped longitudinally, one of the mirrors should have zero reflectance at the pump wavelength λ_p . The other mirror should be a high reflector for the pump radiation to achieve a double pass and therefore a higher absorption efficiency for the pump. A convenient way to realize such a resonator is that one mirror serves simultaneously as input coupler for the pump (zero reflectance) and as output coupler for the waveguide laser emission (optimized reflectivity R_{opt}). The other mirror is just a broad-band reflector for both pump and signal. Therefore, only one mirror has to be dichroic. Pump and signal can be split by an external fiber-optical (f/o) WDM.

Proceeding from these considerations, two laser-resonator parameters are left to be varied for the optimization of the laser performance: the reflectivity of the output coupler for the waveguide laser emission and the length of the cavity. The influence of both was investigated theoretically. For this purpose, the input parameters for the modeling were set according to the properties of the waveguide amplifier described above (e.g., optical modes intensity distributions, waveguide scattering losses, erbium concentration profile). As in the gain measurement, σ -polarized pumping turned out to be most efficient, and this polarization was also assumed for the calculations. According to this, the pump wavelength was set to be 1484 nm, and a coupling efficiency of 85% was taken into account. The reflectivity of the front mirror was set to be $R_1^p = 5\%$ for the pump light, corresponding to the experimental situation which will be described in the following section. For the waveguide laser emission, the reflectance was varied in the range $0.1 \leq R_1^s \leq 0.7$; R_1^s was assumed to be wavelength independent. The resonator length is limited by the length of the given amplifier to a maximum of 7 cm. Nevertheless, we calculated the laser performance for all lengths in the range $3 \text{ cm} \leq l \leq 9 \text{ cm}$. The results of these calculations are shown in Fig. 5 as contour-plots.

The upper left diagram in Fig. 5 shows the expected emission wavelength and polarization of the waveguide laser for all reflectivities R_1^s and resonator lengths l in the ranges given

above. These data were found by calculating the threshold pump power for all possible emission lines and polarizations; lasing will start on the line with the lowest threshold (multi-line emission was not taken into account). Long laser cavities ($l \gtrsim 7$ cm) with low output coupling losses ($R_1^s \gtrsim 0.6$) will exhibit π -polarized laser oscillation at $\lambda_s = 1602$ nm, whereas in shorter resonators with higher losses the laser process can only start on the shorter wavelength lines of Er:LiNbO₃ with higher gain. In very short cavities with high output coupling losses, laser emission only at the line with the strongest amplification ($\lambda = 1531$ nm, σ -polarization) can be expected. The largest existence range is found for σ -polarized radiation at $\lambda_s = 1561$ nm.

These results have been taken into account when calculating the pump threshold, the slope efficiency and the output power for a pump power level of 100 mW, which is a typical value that can be realized with a high-power pump laser diode. The results are shown in the upper right, lower left, and lower right diagrams of Fig. 5, respectively. Here and in the following pump power levels and slope efficiencies are always given with respect to the power incident on the waveguide endface (not coupled pump power). The ranges of different emission wavelength and polarization are indicated in all diagrams. Note that the contour lines at the borders of these ranges are not necessarily continuous. The lowest pump threshold values, highest slope efficiencies, and output powers are observed in the existence range of the σ -polarized emission at $\lambda_s = 1561$ nm. It is not possible to optimize both threshold and slope efficiency simultaneously: minimum thresholds of less than 15 mW incident pump power are predicted for short cavities ($l \lesssim 3$ cm) with high signal output reflectivities ($R_1^s \gtrsim 70\%$). The maximum slope efficiency of $\approx 32\%$ is achieved when the resonator is long ($l \approx 9$ cm) and the signal output coupler has a high transmittance ($T_1^s \approx 20\%$). At the length limit of 7 cm given by the described waveguide amplifier, a slope efficiency of $\approx 30\%$ can still be expected if R_1^s is chosen to be about 30%. Fortunately, this parameter pair (marked by the crosses in Fig. 5) nearly coincides with the point of maximum output power of the waveguide laser at a pump power level of 100 mW (see lower right diagram in Fig. 5). At this point, also the threshold pump power of 22.5 mW is still relatively low; therefore, we decided to use these parameters for the experimental realization of the waveguide laser.

We also modeled the case of π -polarized pumping. As one would expect from the π -polarized amplifier performance, the simulations show that this configuration leads to less efficient waveguide lasers. This is due to the smaller absorption and emission cross sections, the higher waveguide scattering losses, and the worse fiber-to-waveguide coupling efficiency ($\sim 75\%$) for radiation in this polarization. Therefore, we concentrate in the following on the case of σ -polarized pumping.

Consequently, on one endface of the waveguide amplifier, a multilayer dielectric coating was deposited by ion-assisted evaporation. The mirror consists of six pairs of SiO₂-TiO₂ layers quarterwave for 1560 nm, resulting in a peak reflectivity

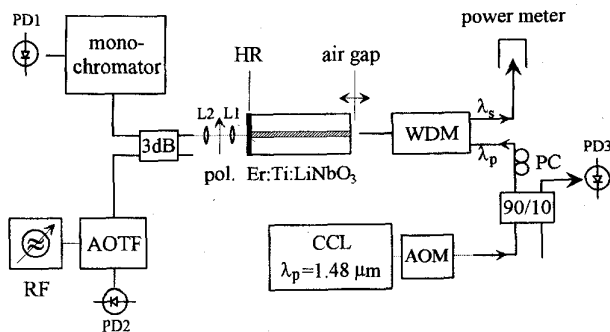


Fig. 6. Setup for the characterization of the Er:Ti:LiNbO₃-waveguide laser. See text for explanation.

of 98%. At the pump wavelength of $\lambda_p \approx 1480$ nm the reflectivity was still $>96\%$. The pump input/signal output coupler was realized in two different ways which will be described in the next sections.

V. LASER CHARACTERIZATION

A. Experimental Setup

The setup for the experimental investigation of the Ti:Er:LiNbO₃-waveguide laser is schematically shown in Fig. 6. The pump input/signal output endface of the sample was uncoated for the first experiments. As a pump source, again the fiber-coupled CCL mentioned above was used. The polarization of the pump radiation was adjusted with a f/o polarizer (PC). 10% of the pump was split off with a f/o 90/10 coupler and monitored with a fiber-pigtailed InGaAs-photodiode (PD3). The main part of the pump light was directed via a f/o WDM to the uncoated endface of the Ti:Er:LiNbO₃ waveguide.

Between the endface of the LiNbO₃ substrate (reflectivity $\approx 14\%$) and the endface of the common fiber of the WDM (reflectivity $\approx 5\%$), a small airgap was left, forming a low-finesse Fabry-Perot resonator. The thickness of this gap and therefore the effective reflectivity of the laser resonator could be adjusted by a piezo-drive in the range $3.5\% < R_{1,\text{eff}}^s < 28.5\%$. The dispersion of the etalon allows one to achieve minimum reflectivity at the pump wavelength simultaneously with nearly any reflectivity for the waveguide laser emission in the range given above. In particular, it is possible to approach the point of maximum output power identified by theory ($\approx 30\%$ reflectivity at $\lambda = 1561$ nm, minimum reflectivity for the pump wavelength). The coupling efficiency was tested to be unchanged by the small gap between fiber and waveguide.

The pump radiation coupled into the waveguide was reflected by the broad-band high-reflector at the rear endface of the sample and therefore passed the laser resonator twice (double-pass pumping). The waveguide laser emission was separated from the residual reflected pump radiation by the WDM and was measured with a power meter. To control wavelength and polarization of the waveguide laser emission, the much weaker output from the rear high reflector was collimated with a 10-mm lens (L1), passed a polarizer, and

was coupled with another 10-mm lens (L2) into one arm of a f/o 3-dB coupler. One half of the signal was directed toward a monochromator for detecting the waveguide laser emission with high spectral resolution ($\Delta\lambda \approx 0.1$ nm). The other half was fed into a fiber-pigtailed polarization independent integrated acoustooptical tunable filter (AOTF) in LiNbO₃ [17] followed by a fiber pigtailed InGaAs-photodiode (PD2). By a repetitive fast scanning of the acoustical frequency, this device could be used as a real-time spectrum analyzer for the wavelength range $1460 \leq \lambda \leq 1600$ nm (resolution ~ 1.2 nm). The repetition frequency of the scans was limited by the RF-generator to ~ 70 Hz.

B. CW Operation

In the first laser experiments, the CCL was operated in a CW mode. Pump wavelength and polarization were set to 1484 nm and $\sigma \hat{=} \text{TE}$, respectively. At the maximum available pump power of about 200 mW from the WDM fiber, laser emission from the waveguide was observed for any reasonable mirror separation of the input/output coupler Fabry-Perot. However, depending on the specific reflectivities of the etalon for pump and laser signal, different emission wavelengths were observed. In Fig. 7, the waveguide laser emission spectrum measured with the AOTF is shown versus the thickness of the airgap between fiber and waveguide endface for an incident pump power of 150 mW. On the right-hand side of the diagram, the corresponding (calculated) effective reflectivities of the input/output coupler for the pump and for the different laser emission wavelengths ($\lambda_s = 1531$ nm, 1546 nm, and 1561 nm, respectively) are given. The experimentally observed existence ranges of these waveguide laser lines are indicated. The detuning of the etalon started from an adjustment where the reflectivity for the pump ($\lambda_p = 1484$ nm) was minimized and maximized for a waveguide laser emission at $\lambda_s = 1561$ nm (etalon thickness change = $0 \mu\text{m}$; absolute etalon thickness about $7 \mu\text{m}$). Indeed, in this configuration, the waveguide laser shows $\sigma \hat{=} \text{TE}$ -polarized emission at $\lambda_s = 1561$ nm wavelength as predicted by the calculations. By reducing the etalon thickness, the output power at this wavelength decreases. Slightly before the point of maximum pump reflectivity and minimum reflectivity at $\lambda = 1561$ nm, the waveguide laser jumps to an emission wavelength of $\lambda_s = 1546$ nm (dark shaded area). Upon reaching this point the laser emission changes to $\lambda_s = 1531$ nm (light shaded area). The maximum output power levels at these emission lines are much smaller than in the case of the 1561-nm laser oscillation. By a further reduction of the etalon thickness the emission wavelength of the Ti:Er:LiNbO₃ laser jumps back to the 1561-nm line, omitting the 1546-nm emission. In all situations, the observed waveguide laser radiation is σ -polarized.

It should be pointed out that scanning the reflectivity of the input/output-coupler etalon does not completely correspond to the situation simulated in Fig. 5. In contrast to the experimental situation, in the theoretical modeling the reflectivity was set to be the same for all possible waveguide laser

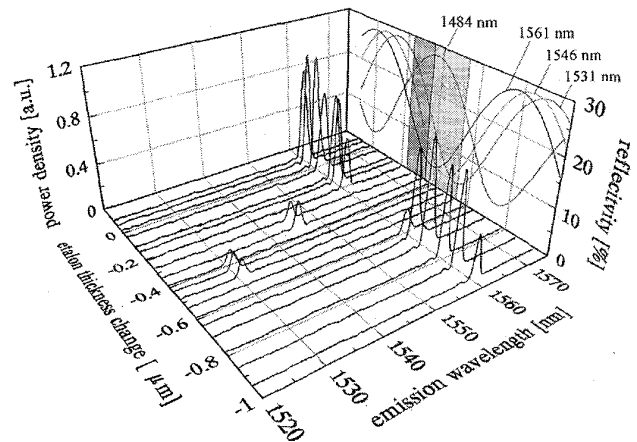


Fig. 7. Emission spectrum of the Er:Ti:LiNbO₃-waveguide laser measured with the AOTF as spectrum analyzer as function of the thickness of the input coupler etalon. Dashed, dash-dotted, dotted, and solid curves: Calculated effective reflectivities of the etalon for pump radiation and three observed waveguide laser emission wavelengths of 1531 nm, 1546 nm, and 1561 nm, respectively. Experimentally observed existence ranges of the different emission lines: White (1561 nm), light (1531 nm), and dark (1546 nm) shaded areas.

emission wavelengths. Additionally, the transmission for the pump radiation was assumed to be unchanged when varying the signal reflectance. Therefore, an absolute agreement of the calculated results in Fig. 5 and the experimental results shown in Fig. 7 cannot be expected. In particular, the dispersion of the input/output-coupler etalon—not taken into account in the calculations—probably is the reason for the observation of the 1546-nm emission, not predicted by the modeling. Nevertheless, it is not yet understood, why π -polarized laser emission at 1531-nm wavelength did not occur.

In the further investigations, we concentrated on the case of maximized output power corresponding to an adjustment of the input/output coupler to minimum pump reflectivity and maximum reflectivity for an emission wavelength of 1561 nm. In Fig. 8, the output power from the uncoated waveguide laser endface is given versus the incident pump power. At a pump power level of 24 mW, laser oscillation sets in. With the maximum available pump power of 210 mW, an output power of 48 mW from the signal arm of the WDM is detected, corresponding to 63 mW in front of the WDM common arm. The power characteristic shows a slight bending with a slope efficiency of approximately 22% for pump powers below 70 mW and $\sim 37\%$ in the upper part of the curve. We have not yet found a reason for this nonlinearity. The power characteristic predicted by the modeling is included in the diagram as a dashed line, showing a good agreement with the measured data: calculated and measured pump power threshold nearly coincide (theoretical value: 23 mW, measured: 24 mW). Also, the calculated slope efficiency of 30.5% shows a reasonable agreement with the measured result. The noise of the power characteristics is mainly due to the instabilities of the CCL pump source.

The case of minimum reflectivity of $\sim 3.5\%$ for pump and waveguide laser emission can easily be obtained by putting a

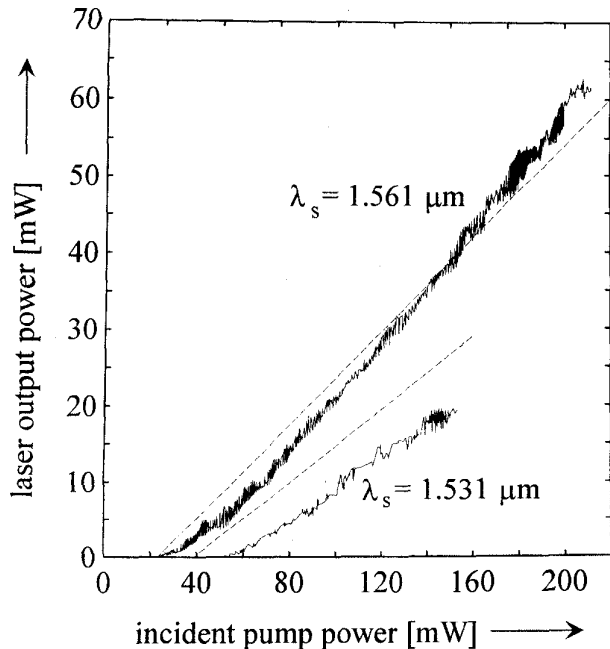


Fig. 8. Waveguide laser output power versus pump power incident on the front face of the chip. $\lambda_s = 1561$ nm: Input/output-coupler etalon adjusted to $\sim 30\%$ for the waveguide laser emission and $\sim 5\%$ for the pump; $\lambda_s = 1531$ nm: $\sim 3.5\%$ reflectivity for both (solid lines: experimental, dashed lines: calculated).

gel, which matches the refractive index of the fiber very well, between the fiber and waveguide endfaces. The waveguide laser emits under this conditions σ -polarized at a wavelength of 1531 nm. The power characteristic for this situation is also given in Fig. 8. The observed pump threshold is ~ 51 mW and the slope efficiency is 21%. At a pump power level of 153 mW, an output power of 19.3 mW is obtained. In this case, the discrepancy with the calculated data, again given as a dashed line, is more significant. The theoretical model predicts a smaller pump threshold of ~ 39 mW. The calculated slope efficiency of $\sim 24\%$ shows a reasonable agreement with the measured data.

C. Pulsed Operation

After the waveguide laser is switched on to a level well above the threshold, it shows pronounced relaxation oscillations which decay after a certain time [11]. When operating the pump laser in a pulsed mode, it is possible just to extract the first, huge pulse from the train of relaxation pulses. Therefore, we ran the Nd:YAG laser, pumping the CCL, in a passively Q -switched mode with an averaged pulse repetition of 43 kHz. A typical CCL pulse and resulting waveguide laser output pulse are shown in Fig. 9. The average pump power incident on the waveguide endface and the average output power of the waveguide laser were 208 mW and 37 mW, respectively (the input/output coupler Fabry-Perot was not fully optimized for maximum output power). The waveguide laser emission was $\sigma \hat{=} \text{TE}$ -polarized with a wavelength of $\lambda_s = 1561$ nm. The pump pulse has a duration of $1.54 \mu\text{s}$ and a peak power of 3.2 W, giving a pulse energy of $5.7 \mu\text{J}$. About $1 \mu\text{s}$ after

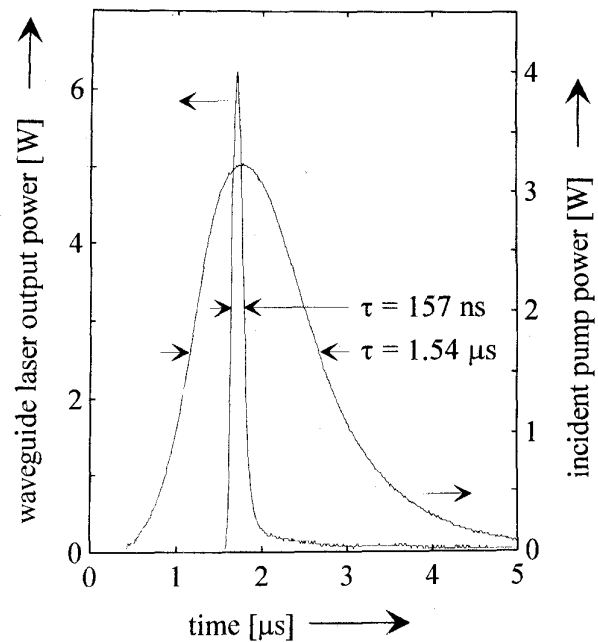


Fig. 9. Waveguide laser output power and incident pump power versus time in a pulsed mode of operation.

the onset of the pump pulse, shortly before its maximum, the waveguide laser emits a 157-ns long pulse with a peak power of 6.2 W and a pulse energy of $1.27 \mu\text{J}$. This result demonstrates that Ti:Er:LiNbO₃-waveguide lasers can be very attractive high-power pulsed light sources.

VI. PIGTAILED AND PACKAGED WAVEGUIDE LASER

A. Mirror Preparation, Pigtailling, and Packaging

To achieve a stable, easy to handle, and easy to operate waveguide laser module, the device had to be pigtailed by gluing a fiber directly to the waveguide endface—without any air gap in between. Therefore, an appropriate coating for the input/output-coupler endface had to be designed. In Fig. 10, the calculated reflectivity of a multilayer dielectric coating between the fiber and the LiNbO₃ endface, consisting of 7 pairs of SiO₂/TiO₂ layers, quarterwave for 1930 nm, is shown as a dashed line. The positions of pump and desired emission wavelengths are indicated by arrows. The mirror was designed to serve as antireflection coating for the pump (calculated reflectivity $< 1\%$ for $1473 < \lambda < 1491$ nm) and as $\sim 30\%$ reflector at the desired emission wavelength $\lambda_s \approx 1560$ nm. For all other possible emission wavelengths of the Ti:Er:LiNbO₃-waveguide laser, the reflectance is lower, so lasing on the longer wavelength lines ($\lambda_s > 1600$ nm) in particular will be suppressed. The coating was fabricated by ion-assisted evaporation of the dielectric layers. It shows a very good agreement with the calculated data: the reflectivity is lower than 1% for $1474 < \lambda < 1495$ nm. The local maximum of the reflectivity is slightly shifted to longer wavelengths: 34% at 1569 nm. The reflectance of 32% at 1561 nm is well within the requested range.

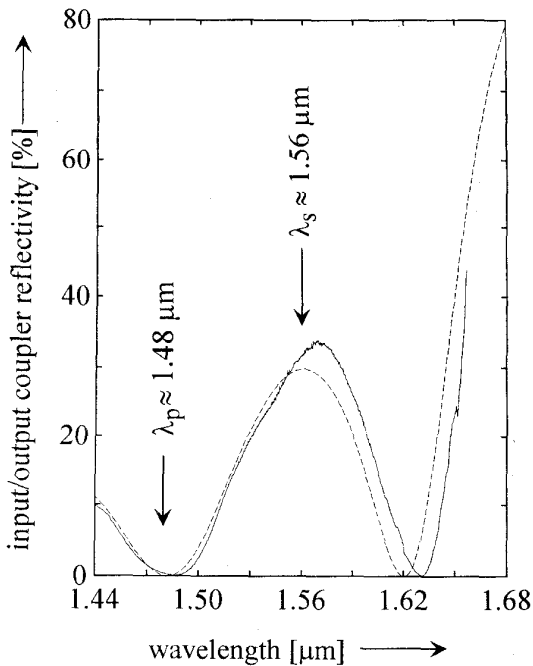


Fig. 10. Reflectivity of the dielectric multilayer mirror (7 pairs $\text{SiO}_2/\text{TiO}_2$, quarterwave for 1930 nm) serving as input/output coupler of the pigtailed waveguide laser versus wavelength (solid line: experimental, dashed line: calculated).

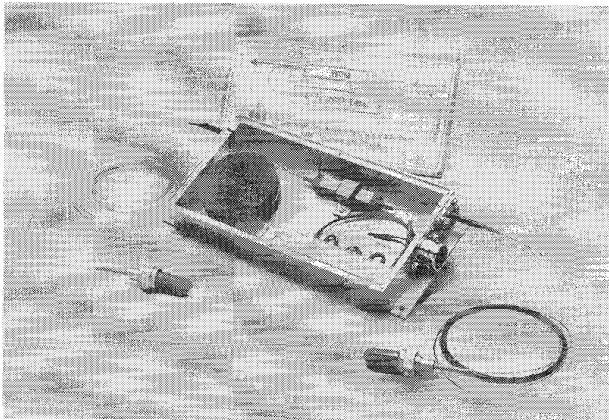


Fig. 11. The pigtailed and packaged waveguide laser module.

The waveguide laser prepared in this way was pigtailed with a standard single-mode fiber directly connected to the common port of a f/θ WDM (type JDS WD1415). Finally, waveguide laser and WDM were packaged into a metal housing including the possibility of temperature control of the LiNbO_3 laser chip (see Fig. 11).

B. Characterization of the Waveguide Laser Module

By adjusting the polarization of the pump radiation appropriately, the waveguide laser module emits with maximum output power at a wavelength of 1562.2 nm with a spectral width of 0.3 nm (FWHM; resolution 0.1 nm). For this

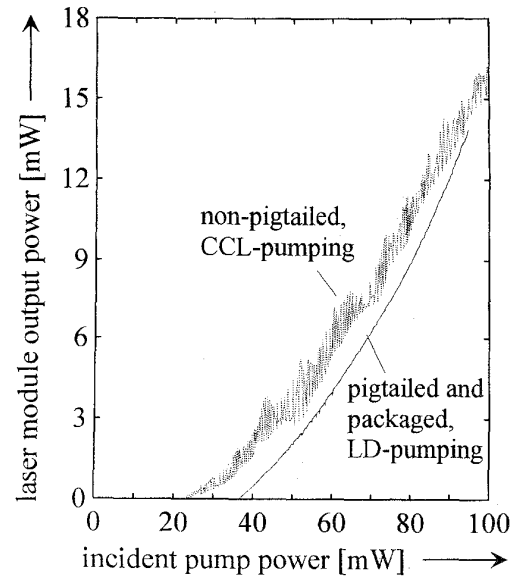


Fig. 12. Output power from the laser diode pumped, pigtailed, and packaged waveguide laser module versus incident pump power. For comparison, the power characteristics of the CCL-pumped solitary waveguide laser chip is included. In contrast to the plot in Fig. 8, here also the losses due to the waveguide-fiber coupling and the WDM are taken into account, resulting in the lower output of the module.

case, the output power from the laser module is shown versus the pump power incident on the waveguide endface in Fig. 12. The mean emission wavelength of the laser diode was adjusted via the device temperature to maximize the pump absorption and therefore the waveguide laser output power at maximum forward current. Consequently, during the scan of the pump power, the mean emission wavelength of the pump shifted from shorter wavelengths to the point of optimum pump efficiency. This results in a higher pump power threshold of 36.6 mW in comparison with CCL pumping of the nonpigtailed sample at the optimum wavelength. Therefore, the corresponding power characteristic has been included in Fig. 12 (in contrast to the plot in Fig. 8, the losses due to the waveguide-fiber coupling and the WDM are also taken into account, resulting in the lower output of the module in comparison with the laser chip alone). At the maximum available pump power of 95 mW from the laser diode, an output power from the waveguide laser module of 14 mW is observed, which is only about 0.5 mW less than for the case of CCL pumping. This shows that the pumping efficiency is nearly the same for the broad-band laser diode ($\Delta\lambda \approx 10$ nm) and the narrowband CCL ($\Delta\lambda \approx 0.2$ nm).

C. Noise Properties of the Waveguide Laser Emission

For the investigation of the waveguide laser emission noise, we directly monitored the output from the laser-diode-pumped and optically isolated laser module with an InGaAs-photodiode.

As mentioned above, the laser shows pronounced relaxation oscillations after switching on. In Fig. 13, the behavior of the laser is shown a long time after the onset of lasing

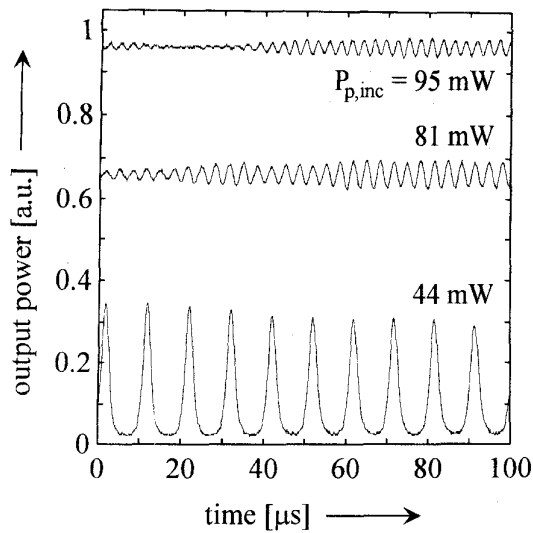


Fig. 13. Output power from the laser-diode-pumped, pigtailed, and packaged waveguide laser module versus time for three different pump power levels.

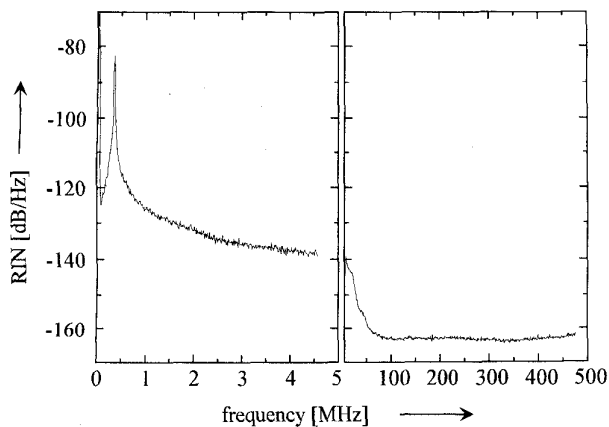


Fig. 14. The RIN of the laser-diode pumped, pigtailed, and packaged waveguide laser module versus frequency for an incident pump power of 95 mW. Left-hand side: Frequency axis stretched by a factor of 100 in comparison to the right-hand side.

for different pump power levels. In all cases, the relaxation oscillations do not decay completely after the onset of lasing. While near the threshold the laser pulses permanently, the amplitude of this oscillation reduces more and more with increasing pump power and approaches a CW behavior with a superimposed (time dependent) small sinusoidal modulation. Its frequency increases with pump power and reaches 350 kHz at the maximum available pump power of 95 mW. Possible mechanisms driving such an oscillation are discussed in [18].

We measured the frequency dependent relative intensity noise (RIN) [19, p. 152] of the waveguide laser module. For this purpose, the AC signal from the photodiode was fed into an electrical spectrum analyzer; the dc current was shortcut with an inductor. In Fig. 14, the RIN is plotted versus frequency for the case of maximum pump power ($P_{p,inc} = 95$ mW). The diagram on the left-hand side shows the low-frequency range with a strong peak of -82 dB/Hz at a

frequency of 350 kHz, corresponding to the residual relaxation oscillations. At higher frequencies, the noise drops very fast. Above 50 MHz, the noise reaches the shot-noise limit, which was ~ -161 dB/Hz. As shown in [20], it is possible to suppress the relaxation oscillation by an appropriate feedback loop to the pump laser power supply.

VII. SUMMARY AND CONCLUSION

In conclusion, the fabrication, characterization, and optimization procedure—including intensive theoretical modeling—for an efficient Ti:Er:LiNbO₃-waveguide laser have been reported. Straight Ti-diffused waveguides were fabricated in an Er-diffusion-doped LiNbO₃ wafer. This sample of 7-cm length was characterized in detail. For example, small-signal gain experiments gave a maximum amplification of 13.8 dB at a coupled pump power of 190 mW. With numerical simulations, it was possible to predict the optimum resonator configuration for a laser assuming the investigated waveguide amplifier as active medium. The validity of the theoretical predictions was verified experimentally. With a 98% and a $\sim 30\%$ reflector for the waveguide laser emission wavelength of $\lambda_s = 1561$ nm, a maximum output power of 63 mW at an incident pump power level of 210 mW (CCL pumping) was obtained. The laser threshold is only 24 mW. A slope efficiency up to 37% was observed. The waveguide laser was pigtailed and packaged. With a high-power 1480-nm laser diode, this module gave a maximum output power of 14 mW at a pump power level of 95 mW. Noise measurements showed that at frequencies above 50 MHz the laser output is shot-noise limited, while at low frequencies around 350 kHz residual relaxation oscillations are observed.

Our future investigations will, on the one hand, concentrate on the suppression of the relaxation oscillations to get a laser output of very low noise. On the other hand, a further optimization of the efficiency seems to be possible. Theoretical calculations predict that a reduction of the scattering losses of the optical waveguides from 0.18 dB/cm by 0.1 dB/cm down to 0.08 dB/cm would increase the maximum slope efficiency from 30.5% up to 44%. Also, a higher erbium doping level and improved overlap of dopant profile and waveguide modes would increase the output power. By replacing one of the dielectric mirrors by a Bragg-reflector single-longitudinal mode, emission will be possible.

REFERENCES

- [1] E. Lallier, "Optically pumped solid state lasers in LiNbO₃," in *Tech. Dig. Integrat. Photon. Res.* Washington, DC: Opt. Soc. Amer., vol. 5, pp. 348–349, 1993.
- [2] W. Sohler, "Erbium-doped waveguide amplifiers and lasers in LiNbO₃," in *Tech. Dig. Integrat. Photon. Res.* Washington, DC: Opt. Soc. Amer., vol. 7, pp. 212–213, 1995.
- [3] R. Brinkmann, W. Sohler, and H. Suche, "Continuous-wave erbium-diffused LiNbO₃ waveguide laser," *Electron. Lett.*, vol. 27, no. 5, pp. 415–416, 1991.
- [4] P. Becker, R. Brinkmann, M. Dinand, W. Sohler, and H. Suche, "Er-diffused Ti:LiNbO₃ waveguide laser of 1563 and 1576 nm emission wavelength," *Appl. Phys. Lett.*, vol. 61, no. 11, pp. 1257–1259, 1992.
- [5] H. Suche, R. Wessel, S. Westenhöfer, and W. Sohler, "Harmonically modelocked Ti:Er:LiNbO₃-waveguide laser," *Opt. Lett.*, vol. 20, no. 6, pp. 596–598, 1995.

- [6] I. Baumann, D. Johlen, W. Sohler, H. Suche, and F. Tian, "Acoustically tunable Ti:Er:LiNbO₃-waveguide laser," *Proc. 20th Europ. Conf. Opt. Commun. (ECOC'94)*, Florence, Italy, 1994, vol. 4, pp. 99-102, post deadline paper.
- [7] J. Söchtig, R. Gross, I. Baumann, R. Brinkmann, W. Sohler, H. Schütz, and R. Widmer, "DBR stripe waveguide laser in erbium-diffusion-doped LiNbO₃," in *Proc. Conf. Opt. Fiber Commun. (OFC'95)*, San Diego, CA, post deadline paper PD11.
- [8] D. Scarano and I. Montrosset, "Modeling of Er-doped LiNbO₃ waveguide lasers," in *Proc. Eur. Conf. Integrat. Opt. (ECIO'93)*, Neuchâtel, Switzerland, 1993, pp. 30-32.
- [9] M. Dinand and W. Sohler, "Theoretical modeling of optical amplification in Er-doped Ti:LiNbO₃ waveguides," *J. Quantum Electron.*, vol. 30, pp. 1267-1276, 1994.
- [10] M. Dinand, "Theoretical modeling of Er-doped waveguide lasers," in *Proc. Workshop on Rare-Earth Doped Optical Waveguides*, B. Jacquier, Ed. France: Les Houches, June 1994.
- [11] M. Dinand and C. Schütte, "Theoretical modeling of relaxation oscillations in Er-doped waveguide lasers," *J. Lightwave Technol.*, vol. 13, no. 1, pp. 14-23, 1995.
- [12] P. W. Milonni and J. H. Eberly, *Lasers*. New York: Oxford Sci., 1985.
- [13] M. Dinand, "Modellierung erbiumdotierter integriert optischer Verstärker und Laser in LiNbO₃," *Cuvillier Verlag, Göttingen*, 1995.
- [14] I. Baumann, R. Brinkmann, M. Dinand, W. Sohler, L. Beckers, C. Buchal, M. Fleuster, H. Holzbrecher, H. Paulus, K.-H. Müller, T. Gog, M. Materlik, O. Witte, H. Stolz, and W. von der Osten, "Erbium incorporation in LiNbO₃," accepted for publication in *Appl. Phys. A*.
- [15] R. Brinkmann, I. Baumann, M. Dinand, W. Sohler, and H. Suche, "Erbium-doped single- and double-pass Ti:LiNbO₃ waveguide amplifiers," *J. Quantum Electron.*, vol. 30, no. 10, pp. 2356-2360, 1994.
- [16] R. Regener and W. Sohler, "Loss in low-finesse LiNbO₃ waveguide resonators," *Appl. Phys. B*, vol. 36, p. 143, 1985.
- [17] H. Herrmann, C. Leifeld, V. Reimann, R. Ricken, U. Rust, W. Sohler, F. Tian, F. Wehrmann, and S. Westenhöfer, "Polarization independent integrated optical, acoustically tunable double stage wavelength filter in LiNbO₃," in *Proc. Europ. Conf. Integrat. Opt. (ECIO'93)*, Neuchâtel, Switzerland, 1993, pp. 14-32.
- [18] C. Schütte, M. Dinand, G. Zumbusch, and R. Brinkmann, "Dynamics of erbium-doped waveguide lasers: Modeling, reliable simulation, and comparison with experiments," *Konrad-Zuse-Zentrum für Informationstechnik Berlin* (publisher), Berlin, Germany, Preprint SC 95-19, 1995.
- [19] K. Petermann, *Laser Diode Modulation and Noise*. Dordrecht, Germany: Kluwer Academic, 1988.
- [20] D. Hiller, R. Corsini, and S. Bosso, "Very low RIN Er:Ti:LiNbO₃-waveguide lasers," in *Proc. 7th Eur. Conf. Integrat. Opt. (ECIO'95)*, Delft, Netherlands, post-deadline papers, 1995, p. 25.

Ingo Baumann was born in Potsdam, Germany, in 1960. He received the diploma degree in crystallography from the Humboldt-University of Berlin, Germany, in 1988 and the Dr.rer.nat. degree from the University of Paderborn, Germany, in 1993.

His dissertation concerned the growth of LiNbO₃ for optical applications. In 1988, he joined the Research and Development Department of Elektronische Bauelemente, Teltow, Germany. There he was engaged in crystal growth and characterization. In 1992, he joined the Department of Applied Physics of the University of Paderborn, Germany. There he was engaged in the technology development of erbium-doped LiNbO₃ waveguide amplifiers and lasers and in material research.

Dr. Baumann is a member of the German Physical Society and the German Society of Crystallography.

Ralf Brinkmann was born in Detmold, Germany, in 1963. He received the diploma degree in physics and the Dr.rer.nat. degree from the University of Paderborn, Germany, in 1988 and 1994, respectively.

His dissertation was on integrated optical amplifiers in Er:LiNbO₃. In 1989, he joined the Department of Applied Physics of the University of Paderborn, Germany. There he was engaged in the investigation of neodymium- and erbium-doped LiNbO₃ waveguide amplifiers and lasers.

Dr. Brinkmann is a member of the German Physical Society.

Manfred Dinand was born in Höxter, Germany, in 1965. He received the diploma degree and the Ph.D. degree, both in physics, from the University of Paderborn, Germany, in 1991 and 1995, respectively.

Since March 1991, he has been a member (Ph.D. student) of the Integrated Optics group of Prof. Dr. W. Sohler in Paderborn. He is working on theoretical modeling of rare-earth doped waveguide amplifiers and lasers.

Wolfgang Sohler (A'88) was born in Wangen, Germany, in 1945. He received the Diplom-Physiker and Dr.rer.nat. degrees in Physics from the University of Munich, Germany, in 1970 and 1974, respectively.

From 1975 to 1980, he was with the University of Dortmund, Germany, working on integrated optics. In 1980, he joined the Fraunhofer Institut für Physikalische Meßtechnik, Freiburg, Germany, as head of the Department of Fiber Optics. Since 1982, he has been with the University of Paderborn, Germany, as Professor of Applied Physics. His research interests include integrated optics, fiber optics and laser physics. He is the (co-) author of more than 100 journal contributions and several book chapters.

Dr. Sohler has been a member of the program committee of several (international) conferences on integrated optics. He is a member of the German Physical Society and of the German Society of Applied Optics.

Susanne Westenhöfer was born in Offenburg, Germany, in 1962. She received the B.E. degree in 1991.

In 1992, she joined the University of Paderborn, Germany, working in research on optical guided wave devices, particularly in chip-to-fiber attachment.